https://doi.org/10.33271/nvngu/2024-4/027

B. T. Ratov[*1],
orcid.org/0000-0003-4707-3322,
V. A. Mechnik[2],
orcid.org/0000-0003-2686-3712,
V. L. Khomenko[3],
orcid.org/0000-0002-3607-5106,
A. O. Ihnatov[3],
orcid.org/0000-0002-7653-125X,
A. B. Kalzhanova[4],
orcid.org/0000-0002-1885-0367

1 – Satbayev University, Almaty, Republic of Kazakhstan
2 – V. Bakul Institute for Superhard Materials of the National Academy of Sciences of Ukraine, Kyiv, Ukraine
3 – Dnipro University of Technology, Dnipro, Ukraine
4 – Yessenov University, Aktau, Republic of Kazakhstan
[*] Corresponding author e-mail: b.ratov@satbayev.university

INFLUENCE OF DISPERSE-HARDENING ADDITIVE CHROME DIBORIDE ON THE STRUCTURE OF CARBIDE MATRIXES OF PDC DRILL BITS

Purpose. Development of highly effective composite diamond-containing materials based on WC–Co matrices with CrB_2 additives with improved mechanical and performance properties for creating matrices of rock-cutting tools for drilling oil and gas wells.

Methodology. The assigned tasks were solved using a comprehensive research method, which includes a review and synthesis of literary sources; conducting analytical studies of existing composite diamond-containing materials; scanning electron microscopy (SEM) methods; X-ray phase analysis methods; calculation of experimental data by the Rietveld method, developed for the characterization of crystalline materials by powder X-ray diffraction; the Williamson-Hall technique.

Findings. It has been established that the structure of the initial 94 %WC–6 %Co composite consists of WC phases with crystal lattice parameters $a = 0.2906$, $c = 0.2837$ nm and graphite with lattice parameters $a = 0.2461$, $c = 0.6708$ nm. The addition of chromium diboride to the composition of the 94 %WC–6 %Co sample leads to the decomposition of the CrB_2 phase and the formation of the final phase composition: WC + B_2CoW_2 + Cgraphite + solid solution of tungsten and carbon in cobalt.

Originality. It was shown for the first time that if the WC–6Co system is characterized by insignificant solubility of the components in each other, then in the WC–Co–CrB_2 system there is a significant mutual dissolution of the components, which leads to a decrease in their sizes during the sintering process. When the threshold concentration (~4 %) of chromium diboride in the charge is reached, phases of the hexagonal WC group and new phases of the orthorhombic group B_2CoW_2 and amorphous carbon inclusions begin to form in the structure of the composite.

Practical value. A highly effective composite diamond-containing material based on WC–Co matrices with CrB_2 additives with increased mechanical (hardness, crack resistance, compressive and bending strength) and operational (wear resistance, productivity) properties has been developed to create a highly effective rock-cutting tool for drilling oil and gas wells.

Keywords: *rock-cutting tool, diamond, composite, tungsten carbide, cobalt, chromium diboride, rock*

Introduction. Over the last decade, there has been a consistent decline in the utilization of roller bits for drilling oil and gas wells. They are being supplanted by bits enhanced with polycrystalline diamond cutters (PDC). These PDC-equipped bits offer similar mechanical drilling rates and, owing to their superior durability, enable the attainment of substantially elevated operational speeds and economic performance in drilling operations [1].

One of the strengths of PDC bits lies in their ability to disintegrate rock material through a shear process, which proves to be more energy-efficient compared to the compressive stresses generated by roller cone bits. In shear, the energy needed to surpass the plastic fracture threshold is notably lower than in compressive stress scenarios. Consequently, PDC bits demand a reduced specific axial load compared to roller cone bits. Consequently, rock fragmentation through shearing consumes only 15–20 % of the energy required for crushing and grinding, granting PDC bits the capacity to drill significantly faster and more effectively than roller bits. Typically, a sharp PDC bit drills two to three times faster than the most proficient roller cone bit in soft formations, albeit its efficacy diminishes gradually with wear and bluntness [2].

The performance and functionality of PDC bits are notably affected by the physical and mechanical attributes of composite diamond-containing materials (CDMs).

CDMs constructed on carbide matrices represent a promising avenue in materials science, delivering substantial enhancements in efficiency across various sectors such as well drilling, mining, and construction. Over recent decades, CDMs have garnered attention from researchers and engineers owing to their distinctive capability to merge the high hardness of diamonds with the robustness and durability of carbide binders. These materials hold the potential to significantly enhance the effectiveness and longevity of drill bits utilized in demanding geological conditions characterized by high pressure, high temperature, and aggressiveness.

CDMs comprise diamond grains, tungsten carbide (WC), cobalt (Co) phases, or their corresponding alloys, alongside a reinforcement phase (carbides, nitrides, borides, etc.) [3].

The properties of CDMs depend on the sintering methods, technological parameters, phase composition, morphology, and microstructure [4].

A primary concern arises from the heterogeneity within the structure of CDM, potentially resulting in an uneven dispersion of diamond particles and subsequently diminishing the overall efficacy of the material [5]. This issue impacts the mechanical and thermal attributes of CDM, thereby imposing significant constraints on their applicability under conditions characterized by high loads and fluctuating temperatures [6]. Moreover, when drilling through hard rock formations, there is a degradation in the strength properties of CDM, including hardness, compressive and bending strengths, fracture toughness, as well as the capacity to securely retain diamond grains (diamond retention) [7], and resistance to wear [8].

It is worth mentioning that numerous CDMs exhibit high brittleness, imposing constraints on their applicability in abrasive and fractured rock formations [9]. Another noteworthy concern pertains to the intricacies involved in the manufacturing process of CDM, particularly considering the need for precision shapes and geometry. Technologies utilized in the production of such materials frequently encounter challenges in crafting intricate structures, consequently restricting their utilization in the manufacturing of high-precision equipment [10].

Enhancing the mechanical and operational characteristics of CDM and the drill bits derived from them represents a crucial scientific objective. Successfully addressing this task will enhance the efficacy of their utilization in challenging rock formations.

Literature review. The research [11] examined the wear resistance of drill bits coated with tungsten carbide, DLC-diamond coating, and titanium-silica-aluminum (TiAlSi) coating during drilling operations in hard rock formations. Drilling experiments were conducted on rectangular specimens using a drilling machine with rotational speeds of 850, 900 and 950 rpm, and penetration speeds of 12, 18 and 24 mm/min. The results revealed that irrespective of fixed drilling conditions, the wear rate of the TiAlSi-coated bit was 48–60 % lower than that of the WC-coated bit. Similarly, the DLC diamond-coated bit exhibited wear rates 42–55 % lower than those of the WC-coated bit in similar rock formations. Furthermore, apart from the observed changes in bit wear rates, the surface roughness achieved by these bits demonstrated the superior performance of the TiAlSi-coated bit. It was noted that as the mechanical properties of the rock increased (uniaxial compressive strength, Mohs hardness, abrasiveness index, and Young's modulus), the tested drill bits exhibited broader variations in wear resistance. This was evident as the TiAlSi-coated bit displayed the lowest wear rate (27 %), while the DLC diamond-coated bit exhibited superior wear performance (30 %) compared to the WC-coated bit (60 %).

The operational effectiveness and longevity of impregnated diamond tools hinge significantly on their wear conditions, particularly the diverse wear modes exhibited by the metal matrix. Given that traditional qualitative descriptions fall short in establishing mathematical relationships, the study [12] employed the Mask R-CNN deep learning approach to quantify die wear based on scanning electron microscope (SEM) images. A series of WC-Cu metal matrix composite (MMC) samples were fabricated through hot pressing and subjected to pin-on-disk wear testing to generate wear surface images and datasets pertaining to normal wear. Following training, validation, and testing on SEM wear image datasets, the wear segmentation results from the trained model demonstrated that Mask R-CNN can automatically and accurately discern metal die wear, aligning well with manually labeled results. Comparative analysis with artificial intelligence statistical outcomes revealed that the average wear zone mask exceeded 70 %, with the average wear zone area loss being less than 3 %. Furthermore, the Mask R-CNN model exhibited robust performance in detecting wear on similar images from published literature.

In pursuit of enhancing the overall performance of brazed diamond joints, tungsten-coated diamonds have been developed as alternatives to conventional uncoated diamonds. In [13], the interfacial bonding characteristics of tungsten-coated diamonds, achieved through induction brazing utilizing a Ni–Cr alloy, were investigated. The presence of tungsten coating led to optimized interfaces in the solder joints, resulting in improved microstructure and a notable reduction in the occurrence of interface cracks. At the interface between the W-coated diamond brazed particle and the Ni–Cr alloy, the morphology of the Cr_3C_2 intermetallic compound appeared disordered and discrete, which contributed to a reduction in internal residual stress and maximum residual compressive stress in W-coated diamond joints by 16.35 %. Additionally, the graphitization and erosion rate of W-coated diamond particles were significantly enhanced. Brazed W-coated diamond bits exhibited exceptional machining performance, with the wear pattern of W-coated diamond particles during drilling being primarily characterized by mild particle microcracks rather than detrimental particle macrocracks or brittle intergranular cracks.

As rocks exhibit varying degrees of abrasiveness owing to their inherent drilling characteristics, the selection of the metal matrix composition must be meticulously tailored to the hardness and abrasiveness of the rock. A primary criterion in this selection process is to ensure a closely matched wear rate between the diamond and the metal matrix, thereby enhancing the tool's cutting performance. Consequently, the objective of [14] was to enhance the cutting efficacy of diamond tools by identifying the appropriate matrix composition contingent upon the hardness and abrasiveness of the rocks being drilled. To this end, two metal matrix compositions based on cobalt (Co) and iron (Fe) were chosen, and comparative analyses of their microstructure, mechanical properties, and wear resistance were conducted. Microstructural, physical, and mechanical assessments were carried out utilizing techniques such as SEM-EDS, XRD, density measurements, hardness measurements, compression tests, and wear tests. Furthermore, the cutting performance of the specimens was evaluated through field trials. The findings revealed that the mechanical properties, hardness, and wear resistance of Co-based matrices surpassed those of Fe-based matrices. Field tests indicated that the Fe-based matrix exhibited greater suitability for cutting marble, whereas the Co-based matrix was more adept at cutting granite.

When employing PDC bits, recurring issues of cutter failure often arise due to residual stress within the PDC cutters. These residual stresses emerge from the material property disparities between the polycrystalline diamond layer and the tungsten carbide substrate post-sintering and cooling processes. In order to mitigate residual stresses within PDC cutters, the design of PDC cutters with a functionally differentiated structure was optimized in [15]. The influence of gradient structural parameters on residual stresses within PDC cutters was analyzed utilizing finite element methods. Findings indicate that as the thickness of the gradient structure layer increases, the maximum residual tensile stress gradually decreases and stabilizes. While the total thickness of the gradient structure layer remains constant, augmenting the number of layers (thereby reducing the thickness of each layer) does not alleviate the maximum tensile stress but does minimize abrupt changes in axial stress at the interface. Optimal design parameters for the gradient structure are proposed, and a graded PDC cutter is fabricated using fused deposition modeling and sintering technology, resulting in a 62 % reduction in maximum shear stress, a 70 % reduction in maximum axial stress, and a 40 % reduction in maximum radial stress compared to conventional PDC cutters. The accuracy of finite element calculations is corroborated by the results of Raman spectroscopy.

In [16], a low-carbon, energy-efficient sintering process with uniform temperature distribution was developed to ad-

dress several challenges encountered during the sintering of drill bits in medium frequency furnaces. These challenges include significant temperature disparities around the circumference, uneven heating of the mold, and low energy efficiency. Theoretical calculations revealed that the conventional drill bit sintering process consumed 12.7 kWh of energy with an energy loss of 8.84 kWh. In contrast, the low-carbon sintering process achieved an energy output of 4.2 kWh with a minimal energy loss of only 0.26 kWh. Consequently, the energy utilization rates for the two processes were 30.4 and 93.8 %, respectively. During experimentation, it was observed that when sintering bits with a diameter of 76/49 mm at insulation temperatures of 900 and 1,080 °C, the temperature difference around the mold circumference was 43.7 and 48 °C, respectively, in the conventional sintering process. Conversely, under the low-carbon, energy-efficient uniform temperature sintering process, the temperature difference around the mold circumference decreased to 8.7 and 11.3 °C, respectively. This indicates a significant reduction in the average temperature difference around the mold circumference by 81.61 % at 900 °C and 76.46 % at 1,080 °C, leading to enhanced bit quality.

In [17], the impact of incorporating chromium diboride (CrB_2) on the grain size of tungsten carbide was examined. A comparative evaluation of the interphase boundary states in the composites led to the observation that the plasma-spark sintering fabrication technique (applied to samples lacking chromium diboride) results in the formation of either large sections of the cobalt matrix or direct contact boundaries between tungsten carbide grains. Conversely, the inclusion of chromium diboride in the initial materials facilitates the development of thin (up to 100 nm) and extended layers of the cobalt matrix, even between small tungsten carbide grains. It has been demonstrated that the presence of CrB_2 in 94 %WC–6 %Co samples contributes to enhanced uniformity in the grain structure, impedes Oswald ripening processes, and serves as a growth inhibitor, leading to an almost twofold reduction in tungsten carbide grains (from 5.6 to 3.4 μm) with a 10 % CrB_2 content.

Unsolved aspects of the problem. The analysis above highlights the significant attention given to the research aimed at enhancing the structure of drill bit matrices in contemporary publications. Various approaches and methods are explored to enhance the performance characteristics of drilling tools. One promising avenue in this regard is the utilization of dispersion-strengthening additive chromium diboride. However, several unresolved issues persist, such as the solubility of components in each other, phase distribution, and the impact of chromium diboride concentration on the structure of carbide matrix composites in PDC drill bits.

Thus, the **purpose of the article** is to create advanced composite diamond-containing materials utilizing WC–Co matrices augmented with CrB_2 additives. These materials are intended to exhibit enhanced mechanical characteristics (including hardness, crack resistance, compressive and bending strength) as well as operational properties (such as wear resistance and productivity). The ultimate goal is to develop matrices suitable for rock-cutting tools used in the drilling of oil and gas wells.

Objectives of the work are:

1. Investigating the microstructure of images to assess how the incorporation of chromium diboride impacts the behavior of phases in carbide matrix composite materials.

2. Examining the influence of chromium diboride additives on the solubility of components within the bit matrix.

3. Performing X-ray diffraction analysis to determine the nature of transformations occurring during the sintering process of carbide matrix samples for PDC drill bits.

Methodology. The designated objectives were addressed through a comprehensive research approach involving literature review and synthesis, analytical studies of existing composite diamond-containing materials, and utilization of advanced techniques such as scanning electron microscopy (SEM) (using TESCAN Mira 3 LMU microscope with a spatial resolution of 1 nm), X-ray phase analysis (performed with Philips X'Pert PRO MRD diffractometer employing CuK α radiation), experimental data calculation using the Rietveld method tailored for characterizing crystalline materials via powder X-ray diffraction, and application of the High Score Pluse program and Williamson-Hall technique.

Results. ***Microstructure of samples.*** Fig. 1 illustrates electron microscopic images depicting a typical microstructure of sintered samples, acquired through the compositional contrast method.

Microstructural analysis revealed that the primary surface area of sample *1*, composed of 94WC–6Co, consists mainly of light gray and dark gray grains averaging ~4–6 μm in size (Figs. 1, *a–c*). Additionally, smaller, relatively uniform black dark areas are sporadically present in minor quantities. Furthermore, pores measuring 0.2–0.4 μm in size are intermittently observed at the grain boundaries, with their volume fraction being relatively low (Fig. 1, *c*). In contrast, in samples *5* and *6* with compositions 92.12WC–5.88Co–2CrB_2 and 90.24WC–5.76Co–4CrB_2, the sizes of light gray and dark gray grains fall within the range of 2.5–3.5 μm, respectively (Figs. 1, *d–h*), whereas in sample *1*, the light gray and dark gray grains are larger, reaching up to 6 μm (Figs. 1, *a–d*). Notably, their surfaces exhibit no micropores and display a periodic relief with well-defined grain boundaries attributed to the influence of chromium diboride.

In the WC–Co–CrB_2 system, notable mutual dissolution of the components is evident. For instance, while the solubility of components is restricted in the WC–6Co system (sample *1*), in the WC–Co–CrB_2 system (samples *5* and *6*), substantial mutual dissolution of components occurs, resulting in a reduction in their sizes during the sintering process. It is noteworthy that all sintered samples incorporating CrB_2 powder additives in the charge exhibit a more homogeneous phase distribution and a more dispersed structure compared to sample *1*.

Energy dispersive microanalysis (EDS) was conducted to ascertain the composition of phases formed during the sintering process. Fig. 2 displays typical electron microscopic images of samples *1, 5* and *6*, acquired with compositional contrast, highlighting the areas of microanalysis. The outcomes of elemental composition determination in weight ratio are presented in Table 1. Sample 1 exhibited the presence of C, O, Co and W (Fig. 2, *a*; Table 1, spectra 1–6).

Examination of the chemical element ratios revealed that tungsten and cobalt are the primary constituents of sintered sample 1, alongside the presence of carbon and oxygen. Moreover, the microstructure of samples *5* and *6* comprises tungsten (tungsten carbide), cobalt, inclusions of chromium diboride, and amorphous carbon (Fig. 2 and Table 1). The detection of oxygen in trace amounts within the composition of the sintered samples indicates that during section production, oxygen is absorbed by locally activated surface areas, leading to subsequent oxidation.

X-ray diffraction analysis. To elucidate the nature of transformations occurring during the sintering process of the samples, Raman studies of their surface were conducted.

The X-ray diffraction patterns of the samples exhibit 2Θ reflections corresponding to several structural phases: hexagonal structure WC (PDF Number 010-89-2727) with crystal lattice parameters $a = 0.2906$, $c = 0.2837$ nm, graphite (PDF Number 000-56-0160) with crystal lattice parameters $a = 0.2461$, $c = 0.6708$ nm, and phases of the orthorhombic structure B_2CoW_2 (PDF Number 010-72-1276). Notably, the X-ray diffraction patterns do not display reflections from the CrB_2 phase. This could be attributed to the formation of a solid solution of tungsten and carbon in cobalt and carbides of the composition $(Cr, W)_xC_y$ (where $x, y > 1$) under the given technological conditions in the WC–Co–CrB_2 system. The pres-

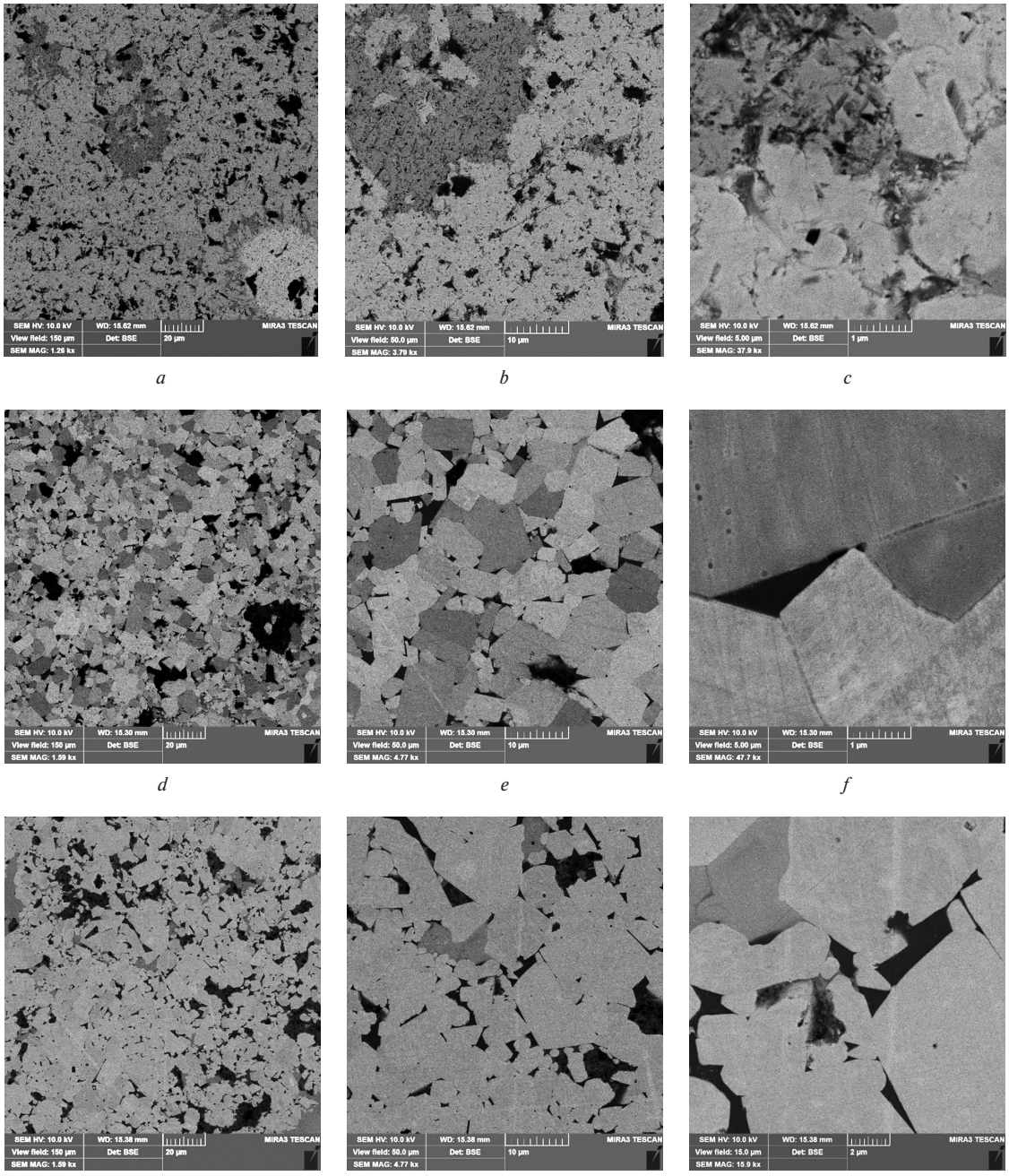

a *b* *c*

d *e* *f*

g *h* *i*

Fig. 1. SEM image of the microstructure of sintered samples:
a, b, c – sample 1; d, e, f – sample 5; g, h, i – sample 6

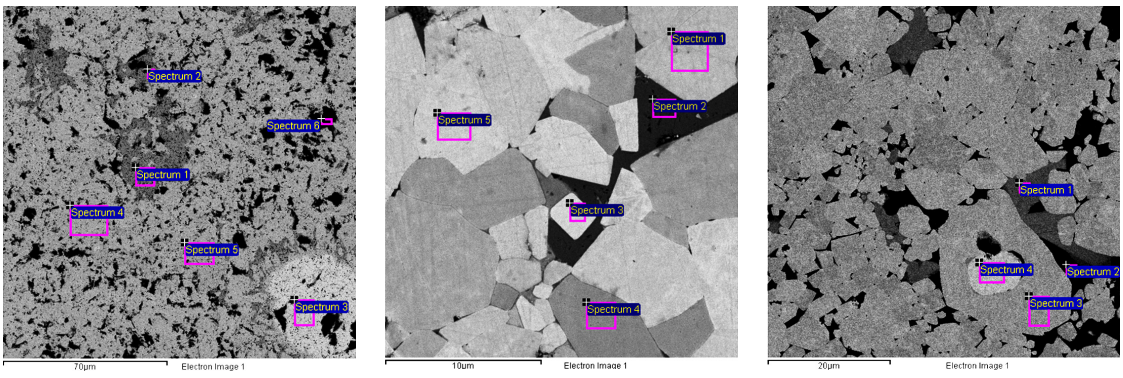

a *b* *c*

Fig. 2. SEM image of the microstructure of sintered samples:
a – sample 1; b – sample 5; c – sample 6

Table 1

Elemental composition of different areas of samples No. 1, 5 and 6, estimated from the analysis of their characteristic X-ray emission spectra

Sample	Spectrum	Content of chemical elements, % (wt.)					
		B	C	O	Cr	Co	W
1	1	–	6.41	1.36	–	17.39	74.83
	2	–	8.11	1.41	–	–	72.21
	3	–	6.76	1.06	–	–	92.17
	4	–	9.79	1.18	–	–	89.03
	5	–	9.58	0.85	–	–	89.57
	6	–	26.10	7.41	–	–	65.20
5	1	–	7.12	5.85	–	–	87.02
	2	3.70	9.64	–	23.62	53.66	9.37
	3	–	8.70	–	–	–	86.22
	4	–	5.03	2.16	–	–	92.81
	5	–	8.89	1.42	–	–	89.69
6	1	5.38	4.24	–	3.37	12.50	74.51
	2	3.65	10.89	–	33.86	42.10	9.50
	3	–	8.81	0.38	–	–	90.80
	4	–	5.57	0.70	–	–	93.73

ence of the B_2CoW_2 phase in the X-ray diffraction pattern suggests the interaction of tungsten and cobalt atoms with boron atoms under high temperature conditions. Analysis of all X-ray diffraction patterns indicates the absence of peaks from any other phases.

Through the examination of X-ray diffraction patterns utilizing the corundum number method, the quantitative content of structural phases in the examined samples was established. The relevant data is presented in Table 2. It should be observed that the reflection parameters for the B_2CoW_2 phase slightly deviate from the tabulated data due to a certain shift.

The results presented in Table 2 allow for an ambiguous interpretation. This ambiguity arises because the addition of chromium diboride to the composition of the examined composites may lead to the formation of a solid solution of chromium in cobalt and carbides of the composition $(Cr, W)_xC_y$ (where $x, y > 1$) [18]. However, this explanation does not fully account for the observed changes in the phase composition and properties of the composites, as CrB_2 in the examined composites serves as a strengthening additive, facilitating the dispersion strengthening mechanism. Furthermore, the release of carbon in the form of graphite inclusions within the composites during operation acts as a lubricant on the working surface, contributing to a reduction in the coefficient of friction and an increase in wear resistance.

Fig. 3 illustrates that the peaks of the B_2CoW_2 phase in samples *7* and *8* are shifted towards higher angles, indicating a decrease in the crystal lattice parameters. The corresponding values of the crystal lattice parameters of the B_2CoW_2 phase, determined from experimental diffraction patterns, are provided in Table 3.

Hence, the sintering process of composite material samples 2–8, containing varying amounts of chromium diboride additives, at a temperature of 1,450 °C induces the decomposition of the CrB_2 phase and the formation of the final phase

Table 2

Phase composition of samples according to X-ray diffraction analysis (wt.%)

Sample	WC, %	Graphite, %	B_2CoW_2, %
1	99.5	0.5	–
2	99.2	0.8	–
3	99.0	1.0	–
4	98.5	1.5	–
5	98.2	1.8	–
6	96.8	1.0	2.2
7	96.6	1.2	2.2
8	96.7	1.1	2.2

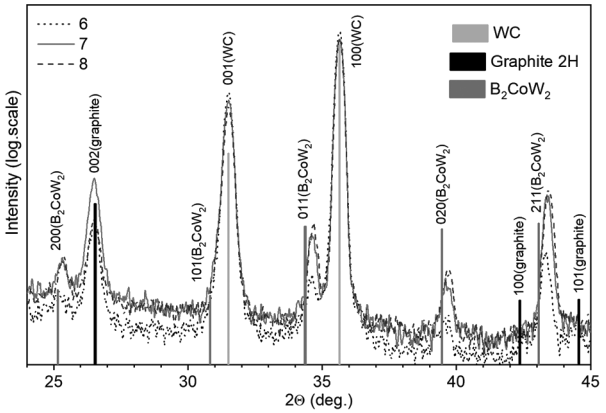

Fig. 3. X-ray diffraction patterns of samples 6 (·····), *7* (——) *and 8* (- - - -); *the peaks of the* B_2CoW_2 *phase for samples 7 and 8 are shifted to the region of large angles*

Table 3

B_2CoW_2 crystal lattice parameters

Sample	*a*, nm	*b*, nm	*c*, nm
6	0.7051	0.4545	0.3181
7	0.7040	0.4542	0.3174
8	0.7032	0.4535	0.3164

composition: WC + B_2CoW_2 + $C_{graphite}$ + solid solution of tungsten and carbon in cobalt. These transformations can potentially influence the physical and mechanical properties of the sintered composites.

Raman spectroscopy. Furthermore, Raman spectroscopy was employed for the characterization of the sintered samples. Fig. 4 displays a series of Raman spectra corresponding to different sections of sample No. 6, which contains 4 % (by mass) of CrB_2, depicted in the upper portion of the figure.

The observed Raman bands can be categorized into two groups: low-frequency bands within the range of 100 to 1,000 cm^{-1}, and bands within the range of 1,300 to 1,800 cm^{-1}. In the high-frequency region of the Raman spectra (Fig. 4, spectra *2*, *5* and *6*) from the dark areas of the sample, bands corresponding to the vibrational modes of the ordered sp^2 phase of carbon are evident [21]. These are known as the D (A1g) and G (E2g) modes, with frequency positions approximately at 1,360 and 1,580 cm^{-1}, respectively. The G band arises from stretching vibrations of bonds within the carbon graphite structure, while the D band is linked to structural disorder. The presence of sp^2 carbon phase clusters in the WC spectra is common, particularly when the material is synthesized using hydrocarbons as precursors (such as methane or acetylene) [22]. Additionally, in certain spectra from the dark areas of the samples where CrB_2 was incorporated, a diamond band of the sp^3 phase with a frequency of about 1,320 cm^{-1} is observed. This signal's emergence is evidently attributed to the remnants of diamond abrasive remaining in areas where amorphous carbon is interspersed between the WC grains.

It is important to highlight that, owing to the sample's component composition, the low-frequency region up to 1,000 cm^{-1} predominantly exhibits vibrating bands associated with tungsten oxide and carbide compounds. Within this range, the most prominent bands can be discerned at 135, 267, 687 and 808 cm^{-1} (spectrum *2* and *6*). A series of bands with

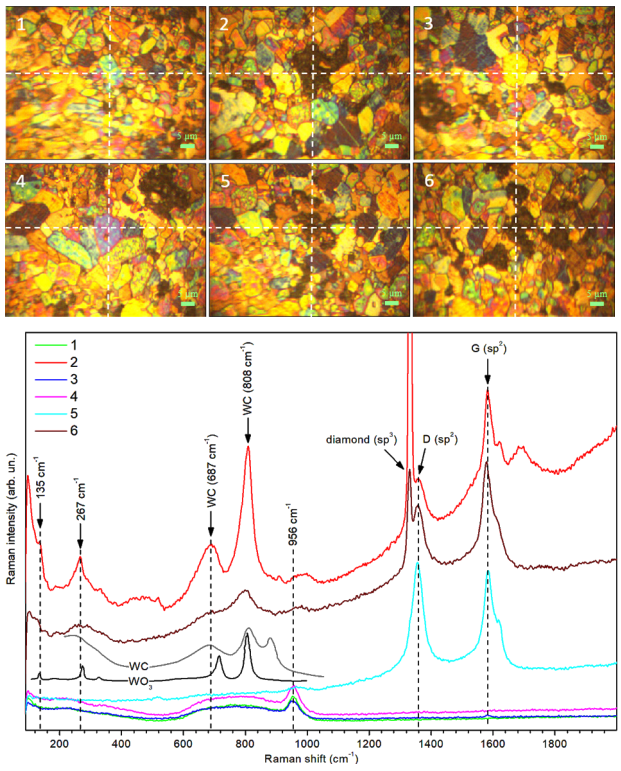

Fig. 4. Optical microimages of the surface and Raman spectra measured in different areas (1–6) of sample No. 6. The spectra of WO_3 [19] *and* WC [20] *are given for comparison. Raman spectra were measured in the central part of each of the images, at the intersection of the dotted lines*

frequency positions of 687, 808, 870 and 965 cm^{-1} are characteristic of Raman scattering in tungsten carbide, representing vibrations of the WC—O/WC, W—C, W=C and W=O bonds [23]. Furthermore, a wide low-frequency band at approximately 250 cm^{-1} is typical for WC.

In terms of Raman scattering in tungsten carbide and tungsten oxide, there exist somewhat conflicting data in the literature concerning the positions and assignment of specific bands. Conventionally, tungsten oxide WO_3 is recognized in its Raman spectrum by bending vibrational W–O modes, peaking at 130, 270 and 330 cm^{-1}, along with stretching W—O vibrations, reaching maxima at 700 and 800 cm^{-1} [24]. For comparison, the spectrum of WO_3 is provided in Fig. 4. Regarding tungsten carbide, in [25], the bands reaching maxima at approximately 700 and 800 cm^{-1} are attributed to vibrations of W—C bonds in titanium carbide. Additionally, in [26], their high-frequency shift with annealing from 685.1 to 692.8 cm^{-1} and from 800.0 to 806.9 cm^{-1} is associated with a change in phase composition from the stable hexagonal α-WC phase to the metastable α-W_2C phase, along with variations in carbon content. It is also emphasized that this behavior differs from the case of monoclinic WO_3, where no shifts of W—O bond bands are observed due to the high stability of the WO_3 phase.

In [27], the bands at 675 and 810 cm^{-1} are similarly ascribed to stretching vibrations of W—C bonds, while the emergence of new bands at 270, 340, 630 and 698 cm^{-1} upon annealing is linked to the oxidation of the WC phase. Slightly varied frequency values were documented in [28], where the band at 801 cm^{-1} was also assigned to W—C stretching vibrations, and three bands at 257, 325 and 700 cm^{-1} were associated with WC oxidation (WC–O bonds). A comparable finding was also reported in [23], where the wear of the WC/C surface of the rotor during operation was investigated. The observed increase in the intensity of the phonon band at 680 cm^{-1} (referred to as WC—O/WC) was linked to WC oxidation, whereas the band at 810 cm^{-1} was attributed to stretching vibrations of W—C bonds without the involvement of oxygen. Consequently, it can be inferred that a series of bands with frequencies of 135, 267, 687 and 808 cm^{-1}, most prominently evident in spectrum 2 (Fig. 4), are associated with the oxidation of tungsten carbide.

In ranges 1, 3 and 4 illustrated in Fig. 4, an extended band is observed around ~760–770 cm^{-1} instead of the bands at 687 and 808 cm^{-1}, alongside a narrower and more pronounced band at 956 cm^{-1}. This spectral behavior in [23] was linked to an escalation in the level of tungsten carbide oxidation during temperature annealing at 1,100 °C, with the band at 956 cm^{-1} attributed to terminal W=O bonds on the surface. The emergence of an additional band around ~960 cm^{-1} in the literature is commonly associated with stretching vibrations of double W=O bonds formed at the grain boundaries of amorphous or nanostructured tungsten oxide [27].

For comparison, Fig. 5 presents Raman spectra corresponding to various sections of sample No. 1, which solely comprised WC and Co.

In this sample, the spectra reveal a broad band peaking around ~240 cm^{-1}, a structural signal spanning the region of 630–870 cm^{-1}, typically lacking a distinct maximum, and a narrower, more pronounced band at 949 cm^{-1}. Similar to the preceding sample, indications of tungsten carbide grain oxidation are observed, particularly the presence of double W=O bonds at the surface and grain boundaries of amorphous or nanostructured tungsten oxide. The low-frequency shift of the W=O bond band to 949 cm^{-1}, alongside a more structured band in the 630–870 cm^{-1} range with characteristic features at 633 and 850 cm^{-1}, suggests a distinction in the structure of amorphous or nanostructured tungsten oxide from the original sample and samples with CrB_2 addition.

Overall, the grains on the surface of the samples (depicted in Figs. 6 and 7) resemble single-crystalline WC inclusions

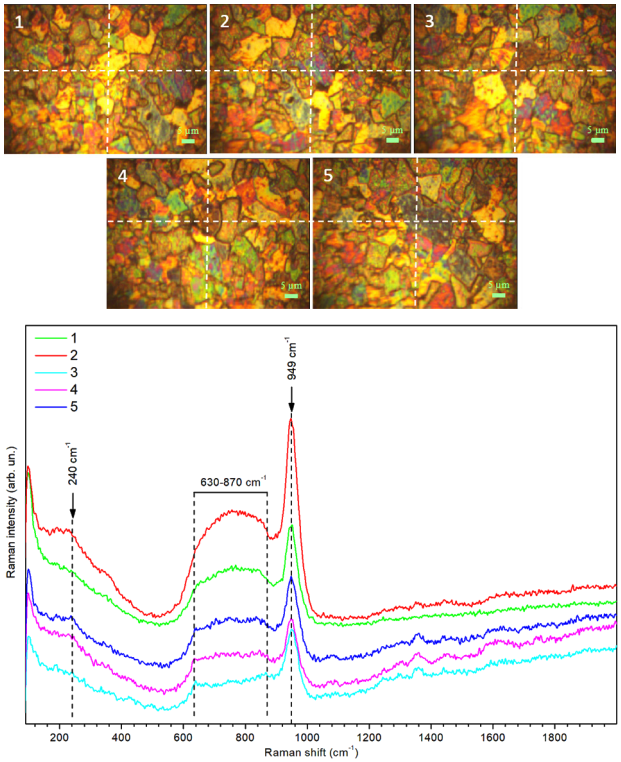

Fig. 5. Optical images of the surface and Raman spectra measured in different areas (1–5) of sample No. 1. Raman spectra were measured in the central part of each of the images, at the intersection of the dotted lines

within a polycrystalline matrix. Similar types of large-sized WC single crystal inclusions were noted during the powder sintering process in the WC–Co system [30]. Throughout the etching process, the grains' surface undergoes varying degrees of oxidation, influenced by the presence of the sp^2 carbon phase on the surface.

Conclusions.

1. The structure of the sintered initial sample comprising 94 %WC–6 %Co is characterized by WC phases (PDF Number 010-89-2727) with crystal lattice parameters a = 0.2906, c = 0.2837 nm, and graphite (PDF Number 000-56-0160) with crystal lattice parameters a = 0.2461, c = 0.6708 nm. The introduction of chromium diboride into the composition of the 94 %WC–6 %Co sample triggers the decomposition of the CrB_2 phase, resulting in the formation of the final phase composition: WC + B_2CoW_2 + $C_{graphite}$ + a solid solution of tungsten and carbon in cobalt.

2. It has been demonstrated that while the WC–6Co system exhibits minimal solubility between its components, the WC–Co–CrB_2 system experiences notable mutual dissolution of the constituents, resulting in a reduction of their sizes during the sintering process. Sintered samples containing CrB_2 powder additives exhibit a more uniform phase distribution and a more dispersed structure compared to samples lacking CrB_2 additives.

3. Upon reaching a critical concentration (approximately 4 %) of chromium diboride in the charge, the structure of the composite starts to exhibit phases from the hexagonal WC group and introduces new phases from the orthorhombic B_2CoW_2 group. Additionally, it initiates the formation of amorphous carbon inclusions within the composite structure. This phenomenon enables the creation of thin (up to 100 nm) and elongated layers of cobalt matrices, even between smaller grains of tungsten carbide.

The study was supported by the Science Committee of the Ministry of Science and Higher Education of the Republic of Kazakhstan (grant No. AP14869271).

References.

1. Sudakov, A., Chudyk, I., Sudakova, D., & Dziubyk, L. (2019). Innovative technology for insulating the borehole absorbing horizons with thermoplastic materials. *E3S Web of Conferences*, *123*, 1-10. https://doi.org/10.1051/e3sconf/201912301033.

2. Wheeler, D. (2018). Applications of diamond to improve tribological performance in the oil and Gas Industry. *Lubricants*, *6*(3), 84. https://doi.org/10.3390/lubricants6030084.

3. Ratov, B., Mechnik, V., Bondarenko, N., Kolodnitsky, V., Khomenko, V., Sundetova, P., ..., & Makyzhanova, A. (2024). Increasing the durability of an impregnated diamond core bit for drilling hard rocks. *SOCAR Proceedings*, *1*, 37-46. https://doi.org/10.5510/OGP20240100936.

4. Ratov, B.T., Mechnik, V.A., Rucki, M., Gevorkyan, E.S., Bondarenko, N.A., Kolodnitskyi, V.M., ..., & Korostyshevskyi, D.L. (2023). $C_{diamond}$–(WC–CO)–ZRO_2 composite materials with improved mechanical and adhesive properties. *Journal of Superhard Materials*, *45*(2), 103-117. https://doi.org/10.3103/s1063457623020107.

5. Dreus, A., Sudakov, A.K., Lysenko, K., & Kozhevnikov, A.A. (2016). Investigation of heating of the drilling bits and definition of the energy efficient drilling modes. *Eastern-European Journal of Enterprise Technologies. Technologies*, *3*(7(81)), 41-46. https://doi.org/10.15587/1729-4061.2016.71995.

6. Ratov, B., Rucki, M., Fedorov, B., Hevorkian, E., Siemiatkowski, Z., Muratova, S., ..., & Bondarenko, N. (2023). Calculations on enhancement of polycrystalline diamond bits through addition of superhard diamond-reinforced elements. *Machines*, *11*(4), 453. https://doi.org/10.3390/machines11040453.

7. Koroviaka, Y., Pinka, J., Tymchenko, S., Rastsvietaiev, V., Astakhov, V., & Dmytruk, O. (2020). Elaborating a scheme for mine methane capturing while developing coal gas seams. *Mining of Mineral Deposits*, *14*(3), 21-27. https://doi.org/10.33271/mining14.03.021.

8. Biletskiy, M.T., Ratov, B.T., Khomenko, V.L., Borash, B.R., & Borash, A.R. (2022). Increasing the Mangystau peninsula underground water reserves utilization coefficient by establishing the most effective method of drilling water supply wells. *News of the National Academy of Sciences of the Republic of Kazakhstan, 5*(455), 51-62. https://doi.org/10.32014/2518-170X.217.

9. Ratov, B., Borash, A., Biletskiy, M., Khomenko, V., Koroviaka, Y., Gusmanova, A., ..., & Matyash, O. (2023). Identifying the operating features of a device for creating implosion impact on the water bearing formation. *Eastern-European Journal of Enterprise Technologies*, *5*(1(125), 35-44. https://doi.org/10.15587/1729-4061.2023.287447.

10. Maksymovych, O., Lazorko, A., Sudakov, A., Hnatiuk, O., Mazurak, A., & Dmitriiev, O. (2021). Stress concentration in bounded compositeplates with carbon reinforcement. *Actual Challenges in Materials Science and Processing Technologies II. Advanced Materials Research*, *1045*, 147-156. https://doi.org/10.4028/www.scientific.net/MSF.1045.147.

11. Piri, M., Hashemolhosseini, H., Mikaeil, R., Ataei, M., & Baghbanan, A. (2020). Investigation of wear resistance of drill bits with WC, Diamond-DLC, and TiAlSi coatings with respect to mechanical properties of rock. *International Journal of Refractory Metals and Hard Materials*, *87*, 105113. https://doi.org/10.1016/j.ijrmhm.2019.105113.

12. Sun, W., Gao, H., Tan, S., Wang, Z., & Duan, L. (2021). Wear detection of WC-Cu based impregnated Diamond Bit Matrix based on SEM image and deep learning. *International Journal of Refractory Metals and Hard Materials*, *98*, 105530. https://doi.org/10.1016/j.ijrmhm.2021.105530.

13. Wang, S., Xiao, B., Xiao, H., & Meng, X. (2022). Interface microstructure and bonding performance of brazed w-coated diamonds using Ni–Cr alloy. *Ceramics International*, *48*(7), 9864-9872. https://doi.org/10.1016/j.ceramint.2021.12.189.

14. Bulut, B., Gunduz, O., Baydogan, M., & Kayali, E.S. (2021). Determination of matrix composition for diamond cutting tools according to the hardness and abrasivity properties of rocks to be cut. *International Journal of Refractory Metals and Hard Materials*, *95*, 105466. https://doi.org/10.1016/j.ijrmhm.2020.105466.

15. Rong, L., Zhang, S., Wu, D., Wu, J., Kong, X., & He, T. (2023). Optimization of functionally graded polycrystalline diamond compact based on residual stress: Numerical Simulation and Experimental Verification. *International Journal of Refractory Metals and Hard Materials*, *117*, 106414. https://doi.org/10.1016/j.ijrmhm.2023.106414.

16. Wang, J., Gao, K., Li, P., & Zhao, Y. (2023). Research on low-carbon, energy-saving sintering process with uniform temperature

for drill bits. *Energies*, *16*(17), 6205. https://doi.org/10.3390/en16176205.
17. Ratov, B. T., Bondarenko, M. O., Mechnik, V. A., Strelchuk, V. V., Prikhna, T. A., Kolodnitskyi, V. M., ..., & Borash, A. R. (2021). Structure and properties of WC–CO composites with different CrB_2 concentrations, sintered by Vacuum Hot Pressing, for drill bits. *Journal of Superhard Materials*, *43*(5), 344-354. https://doi.org/10.3103/s1063457621050051.
18. Kolodnitskyi, V. M., & Bagirov, O. E. (2017). On the structure formation of diamond-containing composites used in drilling and stone-working tools (A review). *Journal of Superhard Materials*, *39*(1), 1-17. https://doi.org/10.3103/s1063457617010014.
19. Vynohradova, O. P., Zakora, A. P., Shul'zhenko, A. A., Gargin, V. G., Sokolov, A. N., Efrosinin, D. V., & Zakora, I. A. (2022). Comparative evaluation of the performance of drill bits with a diamond-containing matrix and inserts made of diamond-containing composites. *Journal of Superhard Materials, 44*(1), 57-61. https://doi.org/10.3103/s1063457622010099.
20. Agudelo-Morimitsu, L. C., De La Roche, J., Escobar, D., Ospina, R., & Restrepo-Parra, E. (2013). Substrate heating and post-annealing effect on tungsten/tungsten carbide bilayers grown by non-reactive DC magnetron sputtering. *Ceramics International*, *39*(7), 7355-7365. https://doi.org/10.1016/j.ceramint.2013.02.075.
21. Maystrenko, A. L., Bondarenko, M. O., Antonyuk, V. S., Petasyuk, G. A., Vinogradova, O. P., Vasylchuk, O. S., ..., & Oleinyk, N. O. (2023). Wear intensity of the functional components made of diamond-containing composite materials during the operation of tools in the process of Rock Destruction. *Journal of Superhard Materials*, *45*(3), 208-216. https://doi.org/10.3103/s1063457623030164.
22. Novikov, V. V., Novikova, O. O., & Bolotov, A. N. (2021). Formation of diamond-containing ceramic abrasive material by microarc oxidation. *Proceedings International Conference "Problems of Applied Mechanics"*. https://doi.org/10.1063/5.0047434.
23. Debus, J., Schindler, J. J., Waldkirch, P., Goeke, S., Brümmer, A., Biermann, D., & Bayer, M. (2016). Indication of worn WC/C surface locations of a dry-running twin-screw rotor by the oxygen incorporation in tungsten-related Raman modes. *Applied Physics Letters*, *109*(17). https://doi.org/10.1063/1.4966145.
24. Lisovsky, A. F., Bondarenko, N. A., & Davidenko, S. A. (2016). Structure and properties of the diamond–WC–6Co composite doped by 1.5 wt % of $CrSi_2$. *Journal of Superhard Materials*, *38*(6), 382-392. https://doi.org/10.3103/s1063457616060022.
25. Novikov, N. V., Maystrenko, A. L., & Prokopiv, N. V. (2012). The formation of diamond-hardmetal granules for the use in rock cutting tools. *Journal of Superhard Materials*, *34*(1), 63-70. https://doi.org/10.3103/s106345761201008x.
26. Song, D., Ren, Z., Yang, Y., Chen, Y., Nie, G., Tan, L., ..., & Zuo, L. (2022). Drilling performance analysis of impregnated micro bit. *Mechanical Sciences*, *13*(2), 867-875. https://doi.org/10.5194/ms-13-867-2022.
27. He, M., Li, N., Zhu, J., & Chen, Y. (2020). Advanced prediction for field strength parameters of rock using drilling operational data from impregnated diamond bit. *Journal of Petroleum Science and Engineering*, *187*, 106847-106847. https://doi.org/10.1016/j.petrol.2019.106847.
28. Dash, T., & Nayak, B. B. (2013). Preparation of WC–W_2C Composites by Arc Plasma Melting and their characterisations. *Ceramics International*, *39*(3), 3279-3292. https://doi.org/10.1016/j.ceramint.2012.10.016.
29. Yang, Q., Yu, S., Zheng, C., Liao, J., Li, J., Chen, L., ..., & Chen, H. (2020). Effect of carbon content on microstructure and mechanical properties of WC-10Co cemented carbides with plate-like WC grain. *Ceramics International*, *46*(2), 1824-1829. https://doi.org/10.1016/j.ceramint.2019.09.158.
30. Pero, R., Maizza, G., Montanari, R., & Ohmura, T. (2020). Nano-Indentation Properties of Tungsten Carbide-Cobalt Composites as a Function of Tungsten Carbide Crystal Orientation. *Materials*, *13*(9), 2137. https://doi.org/10.3390/ma13092137.

Вплив дисперсно-зміцнювальної добавки дибориду хрому на структуру твердосплавних матриць бурових долот PDC

Б. Т. Ратов[*1], *В. А. Мечник*[2], *В. Л. Хоменко*[3], *А. О. Ігнатов*[3], *А. Б. Калжанова*[4]

1 – НАТ «Казахський національний дослідницький технічний університет імені К. І. Сатпаєва», м. Алмати, Республіка Казахстан
2 – Інститут надтвердих матеріалів імені В. М. Бакуля НАН України, м. Київ, Україна
3 – Національний технічний університет «Дніпровська політехніка», м. Дніпро, Україна
4 – Каспійський державний університет технологій та інжинірингу імені Ш. Єсенова, м. Актау, Республіка Казахстан
[*] Автор-кореспондент e-mail: b.ratov@satbayev.university

Мета. Розробка високоефективних композиційних алмазовмісних матеріалів на основі WC-Co-матриць з добавками CrB_2 із підвищеними механічними та експлуатаційними властивостями для створення матриць породоруйнівного інструменту для буріння нафтових і газових свердловин.

Методика. Поставлені завдання вирішувалися комплексним методом дослідження, що включає огляд і узагальнення літературних джерел; проведення аналітичних досліджень існуючих композиційних алмазовмісних матеріалів; методи скануючої електронної мікроскопії (СЕМ); методи рентгенофазного аналізу; облік експериментальних даних методом Рітвельда, розробленим для характеристики кристалічних матеріалів методом порошкової рентгенівської дифракції; методика Вільямсона-Холла.

Результати. Встановлено, що структура вихідного композиту 94 % WC-6 % Co складається з фаз WC із параметрами кристалічної решітки $a = 0{,}2906$, $з = 0{,}2837$ нм і графіту з параметрами решітки $a = 0{,}2461$, $з = 0{,}6708$ нм. Додавання дибориду хрому до складу зразка 94 %WC–6 % Co призводить до розпаду фази CrB_2 і утворення кінцевого фазового складу: WC + B_2CoW_2 + $C_{графіт}$ + твердий розчин вольфраму й вуглецю в кобальті.

Наукова новизна. Уперше показано, що якщо для системи WC-6Co характерна незначна розчинність компонентів один в одному, то в системі WC-Co-CrB_2 має місце суттєве взаємне розчинення компонентів, що призводить до зменшення їх розмірів у процесі спікання. При досягненні порогової концентрації (~4 %) дибориду хрому у складі шихти, у структурі композиту починають формуватися фази гексагональної групи WC і нові фази орторомбічної групи B_2CoW_2 та включень аморфного вуглецю.

Практична значимість. Розроблено високоефективний композиційний алмазовмісний матеріал на основі WC-Co-матриць з добавками CrB_2 із підвищеними механічними (твердість, тріщиностійкість, міцність на стискання й вигин) та експлуатаційними (зносостійкість, продуктивність) властивостями для створення високоефективного породоруйнуючого інструменту для буріння.

Ключові слова: *породоруйнівний інструмент, алмаз, композит, карбід вольфраму, кобальт, диборид хрому, гірська порода*

The manuscript was submitted 18.02.24.